Effects of the bias enhanced nucleation hot-filament chemical-vapor deposition parameters on diamond nucleation on iridium

J. C. Arnault[a] and G. Schull
Commissariat à l'Energie Atomique, Direction des Sciences de la Matière-Département de Recherche sur l'Etat Condensé, les Atomes et les Molecules-Service de Physique et Chimie'des Surfaces et des Interfaces (DSM-DRECAM-SPCSI) Batiment 462, Saclay, 91191 Gif sur Yvette Cedex, France

R. Polini
Dipartimento di Scienze e Tecnologie Chimiche, Università di Roma "Tor Vergata," Via della Ricerca Scientifica, 00133 Rome, Italy

M. Mermoux
Laboratoire d' Electrochimie et de Physico-chimie des Matériaux et Interfaces-l'Ecole Nationale Supérieure d'Electrochimie et d'Electrométallurgie de Grenoble (LEPMI-ENSEEG), Domaine Universitaire, BP 75, 38402 Saint Martin D'Heres Cedex, France

J. Faerber
Groupe Surfaces-Interfaces, Institut de Physique et Chimie de Strasbourg, IPCMS-GSI, Unité Mixte de Recherche (UMR) 7504, BP 43, 23, rue du Loess, 67034 Strasbourg Cedex 2, France

(Received 21 January 2005; accepted 20 June 2005; published online 9 August 2005)

The effects of the bias current density and the filament-to-substrate distance on the nucleation of diamond on iridium buffer layers were investigated in a hot-filament chemical-vapor deposition (HFCVD) reactor. The nucleation density increased by several orders of magnitude with the raise of the bias current density. According to high-resolution field-emission gun scanning electron microscopy observation, diamond nuclei formed during bias-enhanced nucleation (BEN) did not show any preferred oriented growth. Moreover, the first-nearest-neighbor distance distribution was consistent with a random nucleation mechanism. This occurrence suggested that the diffusion of carbon species at the substrate surface was not the predominant mechanism taking place during BEN in the HFCVD process. This fact was attributed to the formation of a graphitic layer prior to diamond nucleation. We also observed that the reduction of the filament sample distance during BEN was helpful for diamond growth. This nucleation behavior was different from the one previously reported in the case of BEN-microwave chemical-vapor deposition experiments on iridium and has been tentatively explained by taking into account the specific properties and limitations of the HFCVD technique. © *2005 American Institute of Physics*.
[DOI: 10.1063/1.1999027]

I. INTRODUCTION

Up to now, iridium is the most promising candidate for diamond heteroepitaxy and highly oriented films have been achieved with weak misorientations as low as 0.6°.[1] This exclusive situation is related to a reduced misfit of 7.6% compared to other heterosubstrates and to the abrupt diamond/iridium interface.[2,3] In comparison, on silicon surfaces, the formation of a β-SiC interlayer leads to ten times larger misorientations and severely limits the oriented nucleation.[1] We previously studied the evolution of the iridium surface during the first stages of the bias-enhanced nucleation (BEN) using the hot-filament chemical-vapor deposition (HFCVD) reactor.[4] In this paper, some of the authors clearly demonstrated that diamond nucleation was promoted only if a BEN step was applied. However, the ratio of oriented with respect to randomly oriented crystals remained poor compared to the BEN-microwave CVD (BEN-MWCVD) technique where the said ratio can be as high as 90%. Independently of the BEN application, the formation of a sp^2 graphitic carbon layer under the CVD environment, a few layers in thickness, was also demonstrated.

The main motivation of the present study was to identify the effects of BEN-HFCVD parameters on the nucleation density, the size distributions of diamond islands, and the ratio of epitaxial crystals. Another purpose was to understand the role played by the graphitic carbon layer on the nucleation mechanism. Thus, samples have been studied by *in situ* auger electron spectroscopy (AES), high-resolution field-emission gun scanning electron microscopy (HR-FEG-SEM), atomic force microscopy (AFM), and Raman spectroscopy investigations.

II. EXPERIMENT

The iridium deposition was carried out using the molecular-beam epitaxy (MBE) technique on $SrTiO_3$, (100)-oriented, single crystals. Films 200 nm thick were grown at 1123 K under a pressure of 4×10^{-8} mbar. The deposition

[a]Author to whom correspondence should be addressed; on leave from IPCMS-GSI UMR 7504, Bât 69, BP 43, 23 rue du Loess, 67 034 Strasbourg Cedex 2, France; FAX: +33-1-69-08-84-46; electronic mail: jcarnault@cea.fr

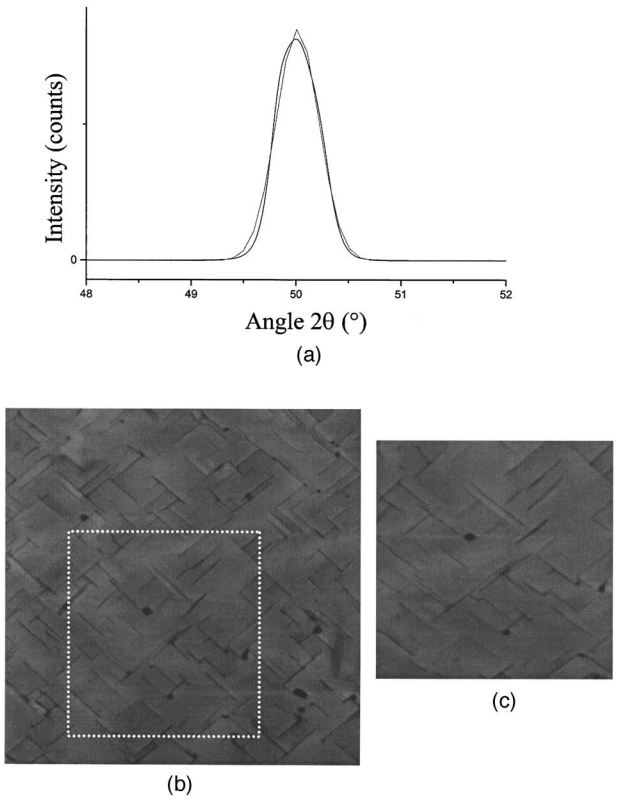

FIG. 1. Characterization of the iridium buffer layers (a) XRD pattern recorded around the Ir (200) diffraction peak. The full width at half maximum (FWHM) is 0.4°. (b) AFM 4-μm^2 image of the iridium surface, the grain boundaries are arranged along the (110) directions. The standard deviation of the height values R_q is 0.52 nm. (c) Enlargement inside the dashed square (1 μm^2).

rate was 4×10^{-2} nm s^{-1}. The texture of the iridium layer was then checked by x-ray diffraction (XRD). The full width at half maximum (FWHM) of the Ir (200) peak was close to 0.4° for the samples used in the present study [Fig. 1(a)]. The morphology of the iridium surface was investigated by AFM. The fourfold symmetry of the grains was well observed on the AFM pictures [Figs. 1(b) and 1(c)]. The grain boundaries were oriented along the (110) directions, their mean depth was close to 0.7 nm according to AFM line scans. The standard deviation of the height values R_q measured on a 4 μm^2 area was 0.52 nm.

The BEN setup installed in our HFCVD reactor was described in detail in a previous paper.[4] Briefly, two electrodes were inserted in the system: the anode was located above the upper tungsten filaments while the cathode was between the two pairs of filaments (Scheme 1). A first negative voltage V_p between the anode and the cathode is applied. Positive ions coming from the gas phase are then accelerated towards the sample surface by applying an extraction voltage V_e between the cathode and the sample. This setup allows the measurement of the sample current I_e collected during the BEN step. From the knowledge of the exposed surface area, the bias current density J_e is then controlled for each experiment.

To grow the diamond samples, a first BEN step was applied before the growth step. Growth was stopped well before the coalescence of the diamond crystallites. The experimental parameters are given in Table I. In the present

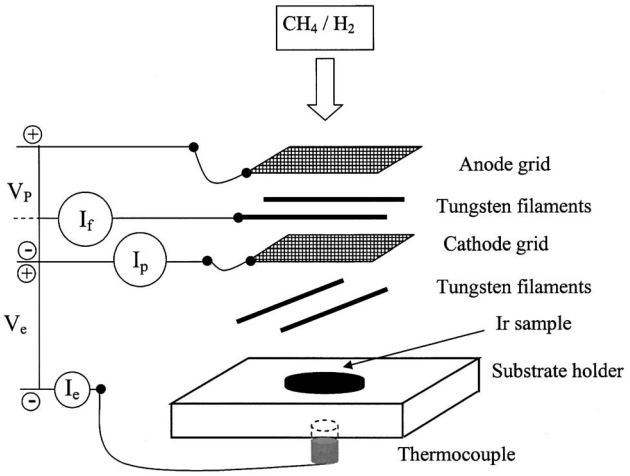

SCHEME 1. BEN-HFCVD system and associated electrical setup. V_P and I_p are bias voltage and plasma current. V_e and I_e are extraction voltage and sample current. I_f is the filament current.

study, the effects of the two main parameters involved during the bias step were investigated: J_e(mA cm^{-2}), the bias current density and d(mm), the distance between the lower tungsten filaments and the iridium surface. First, the bias current density has been varied from 1.4 up to 11.4 mA cm^{-2}. For this set of samples, the distance d was kept to 3 mm. Higher J_e values lead to instabilities of the system. Then, for the upper J_e value, distances of 2 and 4 mm have been used during bias. For the two series of samples, all the other experimental parameters that govern the growth step were kept constant, see Table I. For all the HFCVD runs, the same temperature profile was applied to control the slow rise up to 973 K as well as the cooling at the end of the process.

After the HFCVD process, the reactor was rapidly pumped and samples were immediately transferred into a custom-built vacuum chamber for AES analyses, without any air exposure of the samples. *In situ* surface analyses are known to be powerful tools to investigate the early stages of diamond nucleation on different heterosubstrates, such as silicon,[5] copper,[6] and iridium.[7] This ultrahigh-vacuum (UHV) chamber was equipped with a VSW 100-mm hemispherical analyzer. The base pressure was 10^{-10} mbar in the chamber and 5×10^{-10} mbar during the analysis. The AES spectra were recorded in the derivative mode $dN(E)/dE$ with

TABLE I. Experimental conditions used for the BEN and the CVD steps. The two variable parameters: the filament-to-surface distance d and the bias current density J_e have been underlined.

	BEN step	CVD Growth
CH_4/H_2(%)	5	1
P(mbar)	15	30
Filament activation power (W)	150	185
Filament-to-surface distance (mm)	2–4	5
$T(K)$	973	973
$V_P(V)$	220	-
J_e(mA cm^{-2})	0–11.4	-
Time (min)	30	60

a kinetic energy of the incident electrons of 3 keV and a modulation of 4 V. More details concerning the experimental conditions have been published elsewhere.[5]

High-resolution SEM investigations were performed using either a JEOL 6700F microscope or a LEO Supra 35 both equipped with a field-emission gun providing a high brilliance and a lateral resolution lower than 10 nm for our samples. The images were recorded using an acceleration voltage of 3 or 5 kV. Most of the SEM images were recorded in the secondary electron image (SEI) mode. Nevertheless, several pictures have been acquired by collecting mainly backscattered (BS) electrons using a silicon diode with two sectors. The contrast of the BS image is more sensitive to chemical composition variations of the sample surface.

AFM experiments were carried out at ambient atmosphere with a Dimension 3100 multimode microscope from Digital Instruments. To minimize the interaction with the surface, the vibrating tapping mode was preferred to the contact mode. To improve the lateral resolution and to acquire images of the smaller islands, ultrasharp silicon tips were selected with a 1–2-nm nominal curvature radius. AFM and HR-FEG-SEM investigations were performed within the same areas, because both the techniques allow recording the accurate coordinates of a given region.

Raman spectra were obtained on a Jobin-Yvon T64000 triple monochromator spectrometer equipped with a liquid nitrogen-cooled charge-coupled device (CCD) detector and a microscope. To increase the signal-to-noise ratio, a Notch rejection filter was placed before the entrance slit of a single spectrograph that was equipped with a 1800- or 600-grooves/mm grating. These detection conditions were chosen as a reasonable compromise between spectral resolution and luminosity. A 100× objective was used in all cases. The spot size has been estimated to approximately 0.7 μm from independent measurements conducted on electronic devices. The excitation source was the 514.5-nm line from an $Ar–Kr^+$ laser. Before each analysis, the output laser power has been adjusted to avoid heating or degradation of the samples. Using the present detection conditions, acquisition times of a few seconds (diamond crystallites) or a few hundred seconds (graphitic carbon that was observed on the Ir surface) ensured an acceptable signal-to-noise ratio. To obtain Raman-line scans or images, samples were mounted on an *XY* table movable in 100-nm steps. During the mapping, the full spectra for each point were recorded and stored in an "image file," and images were constructed from the information available in the individual spectra.

III. RESULTS

A. Effects of the bias current density on the nucleation

1. In situ surface analysis

The spectra of the carbon KVV Auger transition are displayed in Figs. 2(a)–2(c) for increasing J_e values: 2.9, 5.7, and 11.4 mA/cm^2, respectively. To make the comparison easier, a reference recorded using a thick diamond film has been added [Fig. 2(d)]. For J_e lower than 5.7 mA/cm^2, the energy positions of the A_i fine structures versus the main minimum are in fair agreement with the highly oriented pyrolytic graphite (HOPG) reference.[4,8] Especially, the well-distinct A_0' fine structure assigned to the $\pi \rightarrow \pi^*$ transition is a clear signature of the carbon sp^2 hybridization. The A_4 fine structure located at 223 eV, still present for Figs. 1(a)–1(c), is a signature of iridium.[9] On the other hand, the spectrum shown in Fig. 2(c) and corresponding to the larger J_e value (11.4 mA/cm^2) exhibited a very different shape, being very similar to the diamond reference [Fig. 2(d)].

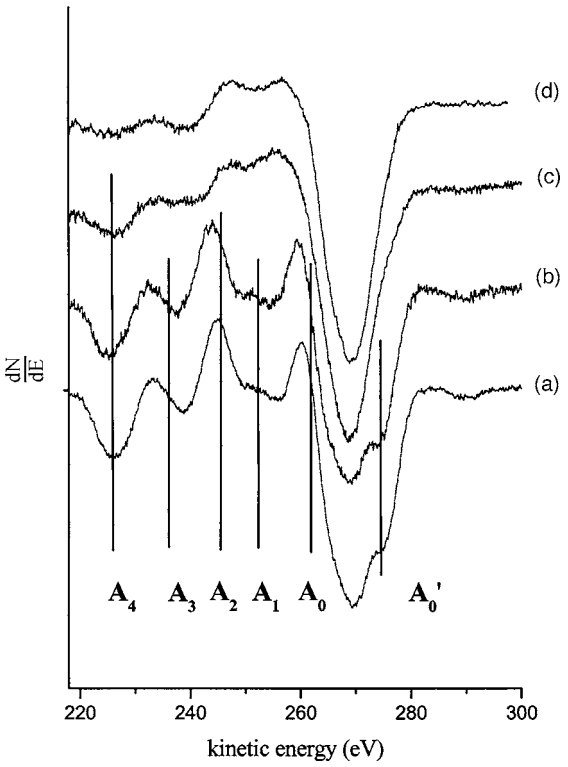

FIG. 2. Carbon KVV Auger transitions for (a) J_e=2.9 mA/cm^2; (b) J_e=5.7 mA/cm^2; (c) J_e=11.4 mA/cm^2; (d) reference spectrum recorded on a complete diamond film. The fine structures $A_i(i=0–3)$ are in agreement with the HOPG reference. A_0' is assigned to the carbon sp^2 hybridization. A_4 is a signature of iridium.

2. HR-FEG-SEM study

The morphology of the iridium surface during the early stages has been previously studied in detail.[4] The high-resolution SEM study focuses mainly on the diamond nucleation density as well as the size distribution functions of diamond crystals. Figure 3 shows the evolution of diamond nucleation density as a function of the bias current density. The main results are also summarized in Table II. It is first observed that no diamond nucleation occurred without a BEN step. This was consistent with a previous work.[4] When the bias current density was raised from 1.4 up to 11.4 mA/cm^2, the nucleation density strongly increased by about three orders of magnitude, from $5\times10^6/cm^2$ to $5\times10^9/cm^2$, see Table II.

Size distributions were obtained from the observation of several hundreds of crystals (Fig. 3). A first result was that the mean size of the crystals was nearly independent of the different bias current densities here investigated: the average particle sizes were 184, 177, and 170 nm for 1.4, 2.9, and

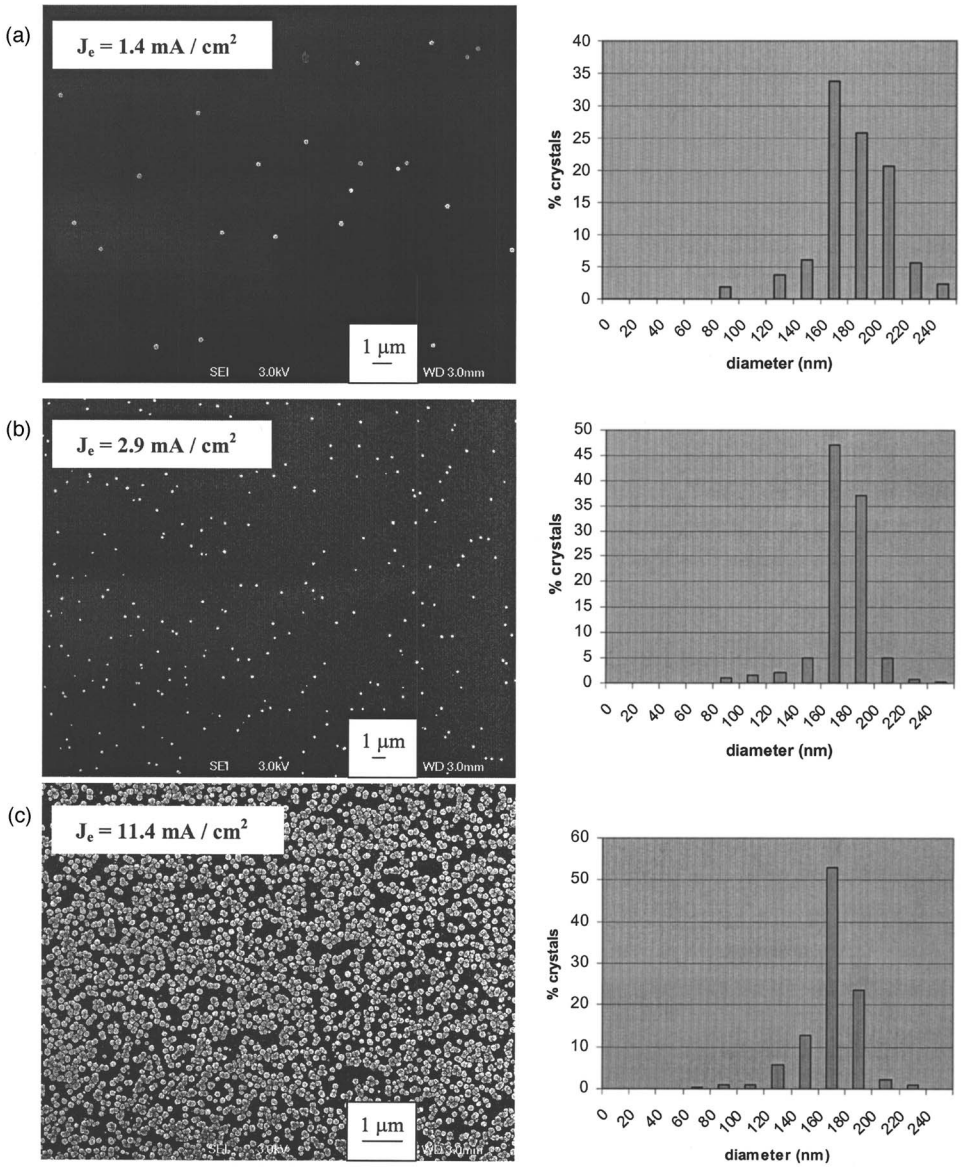

FIG. 3. SEM pictures showing the evolution of the diamond nucleation density with increasing J_e and corresponding size distributions. Mean sizes and standard deviations of the distribution functions are discussed in the text. For all these samples, the distance filaments surface during bias was 3 mm. (a) J_e=1.4 mA/cm^2; (b) J_e=2.9 mA/cm^2; (c) J_e=11.4 mA/cm^2.

11.4 mA/cm^2, respectively. Nevertheless, the size distribution became narrower as J_e was increased. The standard deviations of the distribution functions were 28, 20, and 22 nm for 1.4, 2.9, and 11.4 mA/cm^2, respectively. More than 53% of the crystals have a size included between 160 and 180 nm for 11.4 mA/cm^2 instead of 47% and 34% for lower J_e values. Therefore, higher current density provided both a larger nucleation density and a more homogeneous size distribution function, meaning faster nucleation kinetics.[10] Finally, the orientation of the diamond crystals versus the Ir (100) substrate was poor with a neglectible percentage of heteroepitaxially oriented crystals.

For the case of the higher bias current density, the first-nearest-neighbor distance distribution has been calculated using a previously reported procedure.[10] To achieve this calculation, more than 230 independent observations have been

TABLE II. Diamond nucleation density vs the bias current density (J_e) and the filament-to-surface distance d. The other experimental parameters are given in the Table I. The diamond nucleation densities were estimated from the HR-FEG-SEM pictures.

Bias current density(mA/cm^2)	0	1.4	2.9	5.7	11.4	11.4	11.4
Filaments-sample distance (mm)	3	3	3	3	3	2	4
Nucleation density (/cm^2)	0	5×10^6	10^7	4×10^7	5×10^9	2×10^8	7×10^8

Without BEN, no diamond crystal was observed by HR-FEG-SEM.

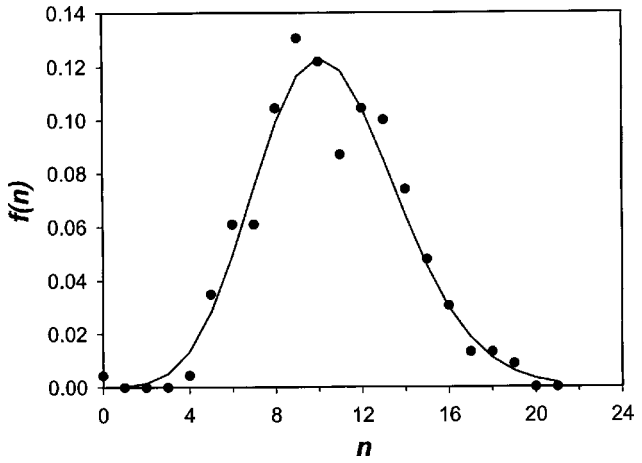

FIG. 4. Number of field of observations containing n particles counted in the sampling disk. The solid line is the Poisson function evaluated using the mean value of particles in the sampling disk and obtained from 230 independent observations.

performed using sampling disks whose radii were between two and four times larger than the average distance between diamond crystals. This former distance was evaluated by the inverse of the square root of the nucleation density. In this case, the average distance between crystals was 510 nm. If the diamond crystals are randomly dispersed on the substrate, the theoretical distribution of the first-nearest neighbors has to follow a Poisson distribution.[10] The plot deduced from the HR-SEM pictures is displayed on the Fig. 4. The comparison of the experimental data with the Poisson distribution function calculated using the mean value of the distribution leads to an excellent agreement. Similar calculations have been repeated on several areas of the sample and a random distribution was always obtained.

B. Effects of the filament-surface distance during bias on the nucleation

1. In situ surface analysis

The spectra of the carbon KVV Auger transition have been recorded for the three d values. For 3 mm, the diamond signature was previously discussed (Sec. III A 1). For 2 and 4 mm, the shape is very close to the one observed on Figs. 2(a) and 2(b), corresponding to a graphitic carbon thin layer signature.

2. HR-FEG-SEM and AFM study

When the distance d between the filaments and the sample was reduced to 2 mm during BEN step, the use of a higher current density (11.4 mA/cm^2) led to a significant drop of the diamond nucleation density, namely, from 5×10^9 to 2×10^8 cm^{-2} (Table II). Moreover, the size distribution function showed a markedly different shape, as evidenced by comparing Fig. 5(a) to Fig. 3(c). It was much broader, with a standard deviation of the distribution function of 90 nm and a mean value close to 350 nm. The only different parameter was the distance between the lower filaments and the substrate surface while BEN and growth durations remained constant. This fact suggests that diamond growth was promoted when the distance was reduced during

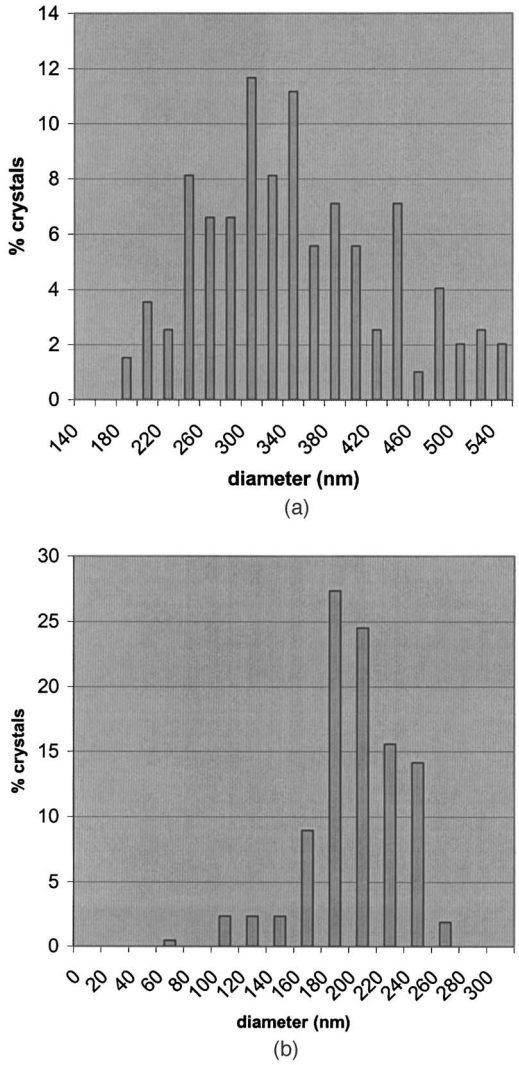

FIG. 5. Size distributions for different distances filaments-surface during bias (a) 2 mm; (b) 4 mm.

the BEN step. This aspect will be further discussed. Coexisting with diamond crystals, small islands were observed with a density of about $7\times10^8/cm^2$. According to AFM pictures, their lateral size was within the range of 55–80 nm and their height was between 22 and 40 nm. As a consequence, they appear brighter on the AFM image [Fig. 6(a)]. HR-FEG-SEM observations carried out in the same area did permit a comparison between images recorded using either secondary or backscattered electrons (Figs. 6(b) and 6(c) respectively). The contrast of the small islands was bright in the SEI mode while it reversed to dark in the images acquired using BS electrons. This behavior was similar to the neighboring diamond crystals[4] which exhibited a high secondary electron emission in SEI and a dark contrast in composition (BS) mode because carbon is a low atomic number element.

When d was increased to 4 mm during bias, the measured diamond nucleation density was $7\times10^8/cm^2$. This value, compared to the 3-mm distance used in Sec. III A, most probably emphasizes the lower efficiency of the ion bombardment to induce the formation of diamond nuclei. For the size distribution, contrary to the previous case, the mean

size of the diamond crystals was 204 nm quite close to the one observed for 3 mm, 170 nm [Fig. 5(b)]. Nevertheless, the size distribution looks broader with a standard deviation of the distribution function of 34 nm for the larger filaments-to-substrate distance.

3. Raman investigations

These three samples have been analyzed using Raman spectroscopy. First, spectra have been systematically acquired between the crystallites that were optically detectable. In agreement with a previous study,[4] as well as with the *in situ* surface analyses, disordered graphite was systematically detected between the crystallites, whose equivalent thickness can be evaluated to a few graphene layers. Second, all the optically detectable crystallites have been identified as diamond. Interestingly, the quality of the spectra was dependent on the analyzed crystallite, meaning that the crystal quality was not constant over the analyzed surface. Statistically, the more perfect crystals were the smallest ones. In this case, a narrow diamond line could be observed on the graphitic signature, without any photoluminescence background. In some cases, the intensity of the graphitic signature was also observed to vary under the diamond crystallites, as described in Fig. 7. Here, spectra were recorded along a line (see the optical image) with 0.5-μm steps. All the spectra exhibited the two graphitic *G* and *D* peaks at about 1350 and 1600 cm^{-1} and the spectrum obtained on the diamond crystallite contains both diamond and graphitic contributions. For this particular case, it is observed that the graphitic signal is stronger under the diamond crystallite, suggesting that diamond nucleates on a graphitic nodule. However, situations for which the graphitic signal intensity did not vary under the diamond crystallite were also observed. For the thickest crystals, broad lines peaking at random in the 1000–1700-cm^{-1} range were observed along with a strong photoluminescence background. The presence of this photoluminescence background which tracks the presence of defects in the crystallites precluded the observation of the surface graphitic signal.

About a hundred of spectra were recorded as an attempt to relate diamond nucleation to changes of the graphitic Raman signature. Given the diameter of the Raman probe (0.7 μm) as compared to the mean crystal size, given the defect content of the thickest crystals, it is still difficult to speculate on the diamond nucleation mechanism.

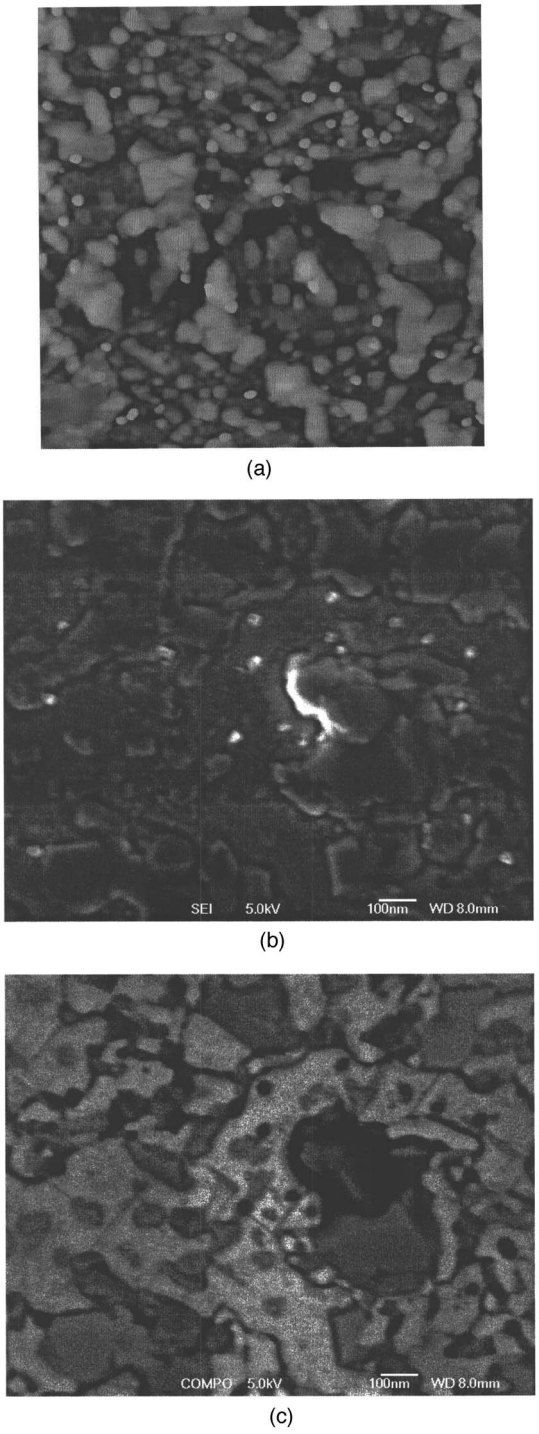

FIG. 6. (a) (2×2 μm^2) AFM image, small islands higher than the surrounding areas exhibit a brighter contrast. (b) HR-FEG-SEM picture showing bright small islands in the SEI mode. (c) These islands appear as dark features in the Composition mode.

IV. DISCUSSION

In this section, we will first discuss what could be the effects of J_c and d on the diamond nucleation, taking into account the role of the graphitic layer. Then, the nuclei ability to grow during BEN will be considered. Finally, the performances of the HFCVD and MWCVD techniques will be compared with a discussion of their intrinsic properties and limitations.

A first result was that the bias step was necessary to provide diamond nucleation. As the bias current density was raised from 1.4 to 11.4mA/cm^2, the nucleation density varied from $5\times10^6/cm^2$ to $5\times10^9/cm^2$ (Table II). It corresponds to a gain of three orders of magnitude. Nevertheless, the bias process employed in our experiments did not lead to any oriented nucleation. The first-nearest-neighbor distribution corresponds to a nucleation that occurred at random on the surface in agreement with a Poisson distribution function (Fig. 4). This behavior is quite different from the one reported for BEN-MWCVD process on iridium[11–13] and silicon.[14] On iridium, diamond-oriented particles are agglomerated forming domains.[11–13] On the other hand, for silicon,

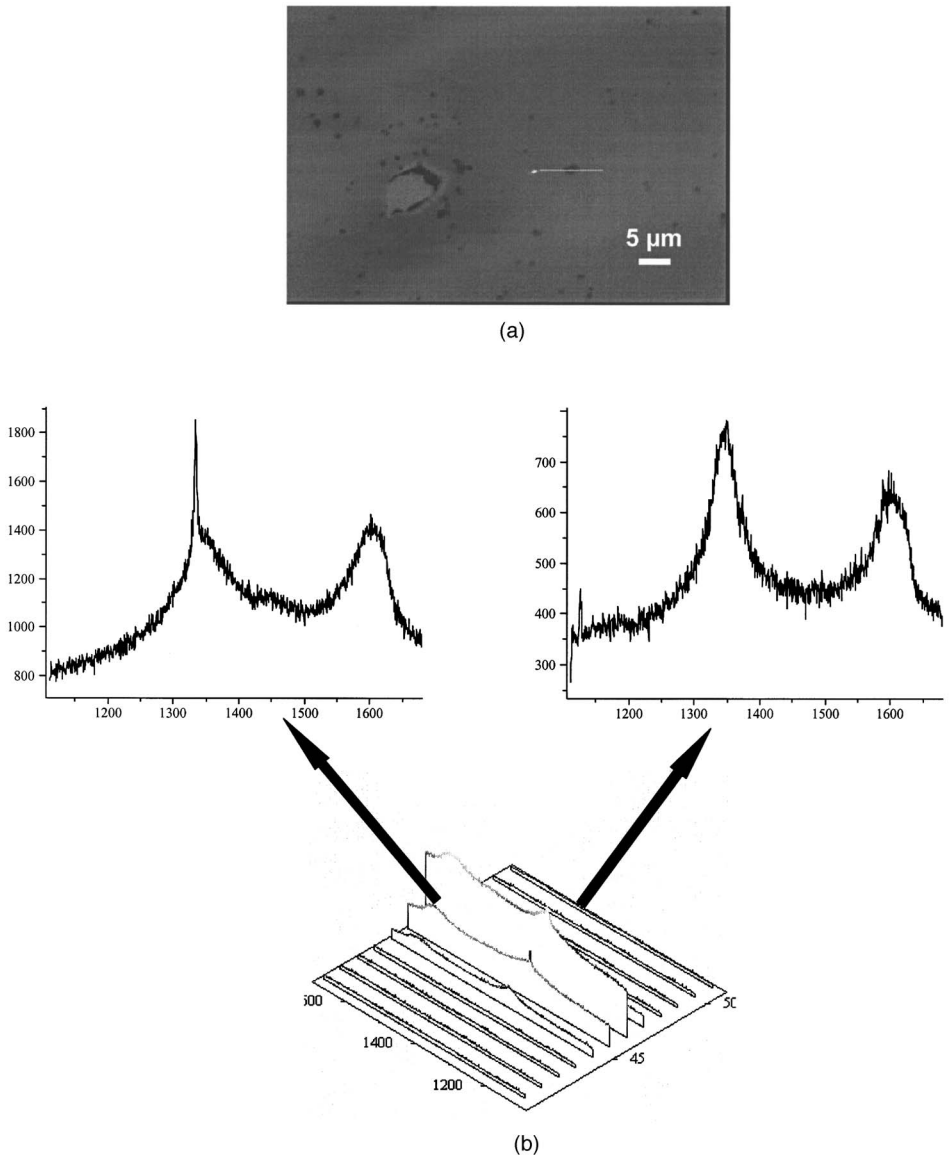

FIG. 7. (a) Raman optical image of the surface for a filament-to-sample distance during the bias of 2 mm. (b) Raman spectra recorded along a line with 0.5-μm step within the same area (the line is displayed on the optical image). Two typical spectra have been enlarged, one is characteristic of the graphitic carbon layer, the other reveals a diamond peak in addition to the two graphitic *G* and *D* peaks.

an enhanced surface mobility of active species during BEN leads to a depletion zone around each diamond nucleus.[14] In the later case, the measured distributions were shifted to larger distances compared to the random case. In the present study, the Poisson analysis of the nearest-neighbor distribution clearly showed that surface diffusion of carbon species on the Ir (100) surface is not the driving force for nucleation during the HFCVD-BEN step.

Indeed, according to our previous *in situ* x-ray photoemission spectroscopy (XPS), Raman and nano-Auger measurements,[4,15] a sp^2 carbon layer was formed over the whole surface during the early stages of BEN. Its thickness corresponded to a few graphitic planes while the in-plane grain size was in the nanometer range. The presence of this carbon layer may support why no direct correlation between the nucleation sites and the Ir (110) directions has been evidenced. In some rare cases only, diamond crystallites exhibiting well-defined (100) facets seem to have nucleated from the iridium surface. Without BEN, diamond nucleation has not been observed with HR-FEG-SEM while graphite formation was demonstrated by AES and Raman.[4] Thus, BEN induces modifications into the graphitic overlayer decisive for diamond nucleation. The kinetic energy of ionic species produced during BEN is sufficient to induce defects within the graphitic layer. Particularly, carbon ions could be subimplanted in the outermost planes of the sp^2 carbon layer[16,17] while the sputtering of carbon atoms is also energetically probable.[15] The irradiation damages could create preferential sites with sp^3 hybridization, suitable for diamond nucleation. This mechanism is well supported by the J_e effect on the nucleation density (Fig. 3). Moreover, this may be in agreement with some of the Raman spectra recorded close to diamond crystallites (Fig. 7) which clearly revealed diamond and graphite contributions. This nucleation route might explain the poor orientation of the diamond crystals with respect to the iridium substrate. However, staring from the Ra-

man results alone, it is still difficult to speculate on the nucleation mechanism.

In opposition to J_e, the use of different d values affects both diamond nucleation and growth. Nucleation densities calculated from HR-FEG-SEM pictures (Table II) remained significantly lower for 2- and 4-mm distances compared to 3 mm. For the shorter distance, 2 mm, particles with a diameter of 60–80 nm were coexisting with diamond crystals, their density was $7\times10^8/\mathrm{cm}^2$ (Sec. III B). As diamond crystals, they exhibited a dark contrast in the HR-FEG-SEM composition mode. Taking into account the two populations of crystals, the total diamond density should be close to $10^9/\mathrm{cm}^2$. This value remains five times smaller than the one obtained for the intermediate distance, demonstrating that the nucleation density is significantly affected. In that situation, the atomic hydrogen concentration at the surface is expected to be larger, as shown by experimental and theoretical studies carried out in similar HFCVD reactors.[18] At short filament-to-substrate distances, the atomic hydrogen concentration profile exhibits a strong increase. A consequence is a more efficient etching of the sp^2 and sp^3 carbon. Even if the etching of sp^2 carbon is considerably faster,[19] nucleation sites could be also negatively affected.[20] For the larger distance of 4 mm, the diamond nucleation density measured from the HR-SEM pictures was seven times smaller than the intermediate value (Table II). When the filament-to-sample distance is increased, the accelerated ions underwent more collisions during their travel through the gas phase. This may support a lower mean kinetic energy for ions impinging the surface and, consequently, a lesser efficiency of the BEN pretreatment.

After the nucleation step, let us now consider the growth mechanism. When the same d value is used during BEN (Sec. III A), the growth mechanism seems to be unchanged. Size distributions exhibited a very close mean size and standard deviations (Fig. 3). On the other hand, a large size dispersion appeared as d is shortened [Fig. 5(a)]. We previously justified the raise of the atomic hydrogen concentration for short filament-surface distances. Consequently, the increase of [H] at the substrate surface leads to a superior recombination rate for atomic hydrogen. This highly exothermic reaction (-104 kcal/mole of H_2) (Ref. 21) induces a significant raise of the surface temperature. The sensitivity of the diamond growth rate to the temperature is well known[19] and may explain the size distributions which show a double mean size [Fig. 5(a)] compared to larger d values [Figs. 3 and 5(b)] using the same conditions for the growth step. Thus, the growth of diamond nuclei begins under bias conditions leading to the wide dispersion of the size distribution. This result is interesting because the ability of the diamond crystals to grow during bias remains an open question for the diamond/iridium system. During the bias step, diamond formation results from a strong competition between etching and nuclei growth mechanisms. On silicon surfaces, diamond nuclei generated during bias can rapidly grow.[1] On the other hand, a SEM study suggested that under standard BEN conditions, diamond nuclei cannot grow but are etched on iridium.[22] Our results strongly suggest that it is effectively possible to promote the growth of diamond nuclei using specific BEN conditions. On the other hand, at larger distances (i.e., 3 and 4 mm), the average sizes of diamond crystals are comparable, 204 nm instead of 170 nm although the size distribution looks slightly wider for the larger distance [Fig. 5(b)].

Diamond was also found in areas where no faceted crystal can be seen by HR-FEG-SEM, probably because of their smaller size. Pictures acquired in the composition mode revealed crystallites of several tens of nanometers ($d=2$ mm). Thus, another question is the creation time of the smaller diamond islands: either during BEN or during the further growth step. If nuclei were formed during bias, it is hardly understandable why they did not grow as large as the diamond crystals under the growth conditions. For $d=2$ mm, the size distribution well emphasizes that the present BEN conditions are helpful for growth [Fig. 5(a)]. As a consequence, these islands may result from a delayed nucleation which could take place at the end of the BEN step, or—most probably—from a heterogeneous nucleation occuring on sites during the growth step.

Let us now discuss the BEN effects between HFCVD and MWCVD reactors starting from their intrinsic differences and the expected consequences on the diamond nucleation. Contrary to MWCVD,[23] the HFCVD technique provides less atomic hydrogen and less ionic species. Consequently, a glow discharge is hardly stable under usual experimental conditions.[24,25] On the other hand, the electron emission has an essential role in the dissociation of hydrogen and hydrocarbon during the BEN-HFCVD step. Moreover, for bias voltage higher than 200 V, it participates to the ignition of a plasma near the surface.[24] Our double bias system is expected to improve both the stability and the reproducibility of the experiments. In the relevant literature, several MWCVD studies demonstrated the deposition of a thin carbon layer at the early stages of the BEN step on iridium.[26,27] Nevertheless, the studies concerning diamond heteroepitaxy on iridium rarely reported the formation of an interlayer at the interface.[2,3] This carbon film has been removed or converted into diamond during the CVD growth.[13] In the HFCVD process, the sp^2 layer formed at the early stages was not so efficiently etched and this fact can be related to the lower concentration of atomic hydrogen available at the surface. As a consequence, oriented growth is achieved more easily in the BEN-MWCVD process because diamond can directly nucleate on the iridium surface. Moreover, the BEN-MWCVD process permits to achieve a more effective ionic bombardment with reported bias current densities up to $100\ \mathrm{mA/cm}^2$,[28] i.e., ten times larger than the BEN-HFCVD.

V. CONCLUSION

The bias current density had a strong influence on the surface density of diamond nuclei formed by BEN in a modified HFCVD chamber. The effect of the filament-to-substrate distance during bias is thought to result from a balance between the bias efficiency and the atomic hydrogen concentration at the substrate surface during the nucleation step. If it is shortened, the recombination of the higher atomic hydrogen concentration at the surface induces a higher temperature that is helpful for growth. If d is larger (i.e., 4 mm) only a

part of the diamond nuclei can grow and reach a size close to 200 nm. Finally, the intermediate distance (i.e., 3 mm) was observed to represent the best compromise for the nucleation density because it allowed to maintain a strong bias effect and sufficient atomic hydrogen concentration at the substrate surface. Moreover, in these conditions, all the created diamond nuclei can grow in the same way.

The graphitic carbon thin film deposited in the early stages of the BEN step is suspected to be involved in the nucleation route. The statistical analysis of the first-nearest-neighbor distribution functions indicates that the diamond nucleated at random on the surface meaning that the surface diffusion of carbon species has no effect. The atomic hydrogen content and the bias current density are lower in the HFCVD technique compared to MWCVD. We believe that the main obstacle to the oriented nucleation of diamond is the presence of the graphitic carbon layer. Further progresses should imply the suppression of this carbon layer formation before diamond nucleation starts.

ACKNOWLEDGMENTS

The authors are grateful to J. Arabski and G. Schmerber for the deposition and the XRD characterization of the iridium films. They also thank Professor M. Tomellini for fruitful discussions.

[1]M. Schreck, F. Hörmann, H. Roll, T. Bauer, and B. Stritzker, New Diamond Front. Carbon Technol. **11**, 189 (2001).
[2]F. Hörmann, H. Y. Peng, Th. Bauer, Q. Li, M. Schreck, Y. Lifshitz, S. T. Lee, and B. Stritzker, Surf. Sci. **513**, 525 (2002).
[3]F. Hörmann, Th. Bauer, M. Schreck, S. Gsell, and B. Stritzker, Diamond Relat. Mater. **12**, 350 (2003).
[4]J. C. Arnault, F. Vonau, M. Mermoux, F. Wyczisk, P. Legagneux, Diamond Relat. Mater. **13**, 401 (2004).
[5]J. C. Arnault, L. Demuynck, C. Speisser, and F. Le Normand, Eur. Phys. J. B **11**, 327 (1999).
[6]L. Constant, C. Speisser, and F. Le Normand, Surf. Sci. **387**, 28 (1997).
[7]J. C. Arnault, F. Vonau, J. Faerber, J. Arabski, G. Schmerber, F. Wyczisk, and P. Legagneux, Phys. Status Solidi A **199**, 27 (2003).
[8]J. J. Dubray, C. G. Pantano, and W. A. Yarbrough, J. Appl. Phys. **72**, 3136 (1992).
[9]*Handbook of Auger Electron Spectroscopy*, 2nd edition, edited by L. E. Davis, N. C. MacDonald, P. W. Palmberg, G. E. Riach, and R. E. Weber (Perkin-Elmer Corp., Eden Prairie, MN, 1978).
[10]R. Polini, M. Tomellini, M. Fanfoni, and F. Le Normand, Surf. Sci. **373**, 230 (1997).
[11]M. Schreck, Th. Bauer, S. Gsell, F. Hörmann, H. Bielefeldt, and B. Stritzker, Diamond Relat. Mater. **12**, 262 (2003).
[12]T. Fujisaki, M. Tachiki, N. Taniyama, M. Kudo, and H. Kawarada, Diamond Relat. Mater. **12**, 246 (2003).
[13]B. Golding, C. Bednarski-Meinke, and Z. Dai, Diamond Relat. Mater. **13**, 545 (2004).
[14]X. Jiang, K. Schiffmann, and C. P. Klages, Phys. Rev. B **50**, 8402 (1994).
[15]J. C. Arnault, F. Vonau, F. Wyczisk, and P. Legagneux Diamond Relat. Mater. **13**, 261 (2004).
[16]J. Robertson, Diamond Relat. Mater. **4**, 549 (1995).
[17]S. Uhlmann, Th. Frauenheim, and Y. Lifshitz, Phys. Rev. Lett. **81**, 641 (1998).
[18]K. Tankala and T. DebRoy, J. Appl. Phys. **72**, 712 (1992).
[19]K. E. Spear, J. Am. Chem. Soc. **72**, 171 (1989).
[20]J. W. Kim, Y. J. Baik, and K. Y. Eun, Diamond Relat. Mater. **1**, 200 (1992).
[21]W. A. Yarbrough, K. Tankala, M. Mecray, and T. Debroy Appl. Phys. Lett. **60**, 2068 (1992).
[22]F. Hörmann, M. Schreck, and B. Stritzker, Diamond Relat. Mater. **10**, 1617 (2001).
[23]S. Katai, Z. Tass, G. Hars, and P. Deak, J. Appl. Phys. **86**, 5549 (1999).
[24]W. L. Wang, G. Sanchez, M. C. Polo, R. Q. Zhang, and J. Esteve, Appl. Phys. A: Mater. Sci. Process. **65**, 241 (1997).
[25]I. Gouzman and A. Hoffman, Diamond Relat. Mater. **7**, 209 (1998).
[26]T. Tsubota, M. Ohta, K. Kusakabe, S. Morooka, M. Watanabe, and H. Maeda, Diamond Relat. Mater. **9**, 1380 (2000).
[27]Th. Bauer, M. Schreck, F. Hörmann, A. Bergmaier, G. Dollinger, and B. Stritzker, Diamond Relat. Mater. **11**, 493 (2002).
[28]T. Fujisaki, M. Tachiki, N. Taniyama, M. Kudo, and H. Kawarada, Diamond Relat. Mater. **12**, 246 (2003).